Multimodal Chemical Imaging for Linking Adhesion with Local Chemistry in Agrochemical Multicomponent Polymeric Coatings

Alison A. Pawlicki,[1,2,3]*‡ Nikolay Borodinov,*[2,3]*‡ Nicola Giri,*[4] *Sam Moore*[4] *Chance Brown,*[1,2,3]
Alex Belianinov,[2,3] *Anton V. Ievlev,*[2,3] *Olga S. Ovchinnikova*[2,3*]

1. The Bredesen Center, University of Tennessee, 821 Volunteer Blvd., Knoxville, TN 37996, USA

2. Center for Nanophase Materials Sciences, Oak Ridge National Laboratory, Oak Ridge, TN 37830, USA

3. The Institute for Functional Imaging of Materials, Oak Ridge National Laboratory, Oak Ridge, TN 37831

4. Syngenta Crop Protection, 410 Swing Road, Greensboro, North Carolina 27409, USA

KEYWORDS

agricultural production, polymer coating, seed coating, force volume mapping, time of flight mass spectrometry, chemical imaging, atomic force microscopy

ABSTRACT

Seed coatings improve germination and offer higher crop yields through a blend of active ingredients (such as insecticides and fungicides), polymers, waxes, fillers, and pigments. To reach their full potential, fundamental formulation challenges bridging structure and function need to be addressed. In some instances, during industrial-volume packing and transportation, coated seeds do not flow well through elevators, conveyers, and applicators which may reduce yield, and add cost. In this work, we illustrate a combinatorial chemical imaging approach to study seed coatings at the microscale to link chemical and physical properties responsible for low seed flowability. The local chemical composition was examined using Time of Flight Secondary Ion Mass Spectrometry (ToF-SIMS) and at comparable length scales, the local adhesive properties were examined using Atomic Force Microscopy (AFM) force volume mapping. The link between the chemical and the adhesive properties was established by Nonnegative Matrix Factorization (NMF). The correlative multimodal imaging approach developed here utilizing AFM force volume mapping, ToF-SIMS chemical mapping, and data analytics offers a path for linking function with localized chemistry when investigating multicomponent soft material systems.

The functional response of agrochemical seed packaging and coatings are commonly evaluated using bulk characterization techniques.[1-4] However, the functionality of these materials is often driven by chemical and physical phenomena at the micron and nanoscale which is characteristic for polymer-containing mixtures.[5-8] Therefore, coupling multiple high-resolution imaging modalities that link functional and chemical properties at these scales offer an opportunity to understand how the local chemistry drives the physical phenomena. This link is critical for the development of the next generation of agricultural products. The materials used for seed coatings specifically, are a complex blend of binders, fillers, pigments, and active ingredients that serve to improve handling, protection, and facilitate germination.[5,9-14] One critical consideration for coating stability, germination, and insect control is the flowability of coated seeds during packing and transport.[1,5,11-13] A trade-off between the efficacy of the coating, the ease of transport and distribution presents a significant industrial challenge, making brittle or overly adhesive coatings undesirable.[4,15]

Typically, seed coating performance is studied macroscopically in bulk where the standard measurements include the Heubach method, or rates of emptying seed hoppers.[1,3,16] In addition, localized studies of mechanical properties such as adhesion and friction have been carried out to probe the details of the inter-particle contact.[17-20] However, complex interactions such as mixing, aggregation, separation, and chemical bonding that can alter the final performance of the product,[6,7,21,22] are complex and detailed investigation has been missing in agrochemical coatings. Many of the side-effects are rooted in the chemical interactions at the microscale. Therefore, conventional approaches offer little empirical relation between the seed coating and product performance. Thus, to decouple fundamental properties and evaluate their effects macroscopically, coated seeds need to be studied at the length scales of these interactions.

In this paper, we correlate the chemical signatures of seed coating components characterized *via* Time of Flight Secondary Ion Mass Spectrometry (ToF-SIMS), with physical properties obtained by Atomic Force Microscopy (AFM) force volume mapping. This combinatorial analytical approach provides a detailed investigation to relate seed coating formulation with function at relevant scales by mapping the microscale surface adhesion with AFM[23-25] and, at the same length scale, mapping the microscale chemical composition with ToF-SIMS.[26] Correspondingly, we relate the adhesive properties at the microscale to macroscale observations of seed flowability. Three industry relevant corn seed coating formulations containing polymers, waxes and inorganic fillers were used to illustrate a relationship between the macroscopic seed flow, microscale adhesion, and chemical distribution of active and passive ingredients on surfaces. Adhesion data from AFM combined with the chemical profile from ToF-SIMS for each of the coating reveals the relative contributions of each coating component to coverage, chemical heterogeneity, and localized adhesion. The approach reported here establishes a base for predictive analytics and rational design of the multicomponent functional coatings relevant to agrochemical manufacturing.

Results and Discussion

Adhesion Mapping

We examine three industry supplied seed coatings, designated A, B, and C. These vary in their macroscopic flowability performance. Coating A does not flow well through hoppers, coating B flows moderately well, and coating C demonstrates the best flowability. To understand these observations to in terms of microscale properties, AFM force volume mapping was used to map the mechanical properties.[23-25] The adhesion force was extracted from representative 40 μm × 40 μm areas from all coating samples. The adhesion force map for coating C is shown in Figure 1 along with sample Force Distance (FD) curves. The adhesion force maps for all three coatings are shown in Figure S1 in Supporting Information The relative adhesion trend, from highest to lowest, is coatings A, B, and C; with A exhibiting highest adhesion, and C lowest. This corroborates industry determined flowability trends in large volume packing and shipping. More interestingly, the adhesion maps revealed domains of high, intermediate and low adhesion. Since the topography and roughness amongst the three samples is similar (Figure S2 in Supporting Information), this suggests that the mechanical properties are largely associated with different chemical formulations and, likely, variations in local chemical composition.

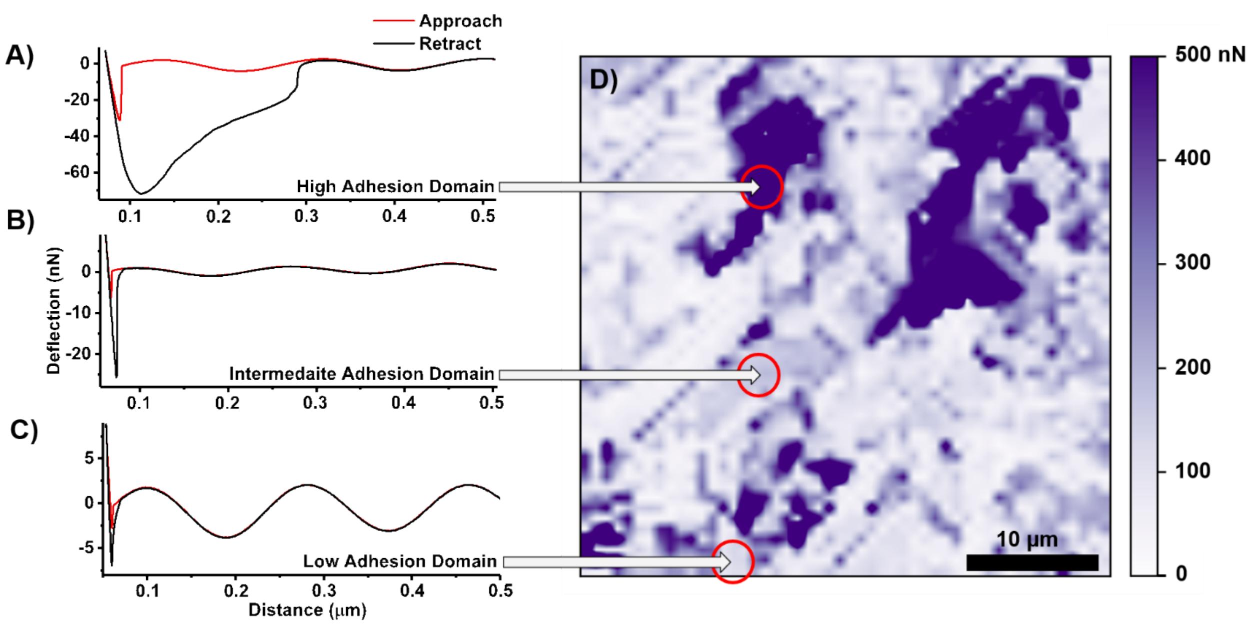

Figure 1. Adhesive properties of corn coating A supported by a glass substrate obtained with AFM force volume mapping. A) FD curve collected on a relative high adhesion domain of the corn coating surface. B) FD curve collected on a relative intermediate adhesion domain of the corn coating surface. C) FD curve collected on a relative low adhesion domain of the corn coating surface. D) Representative adhesion map, acquired from FD curves at 50 × 50 points within a 40 μm × 40 μm area on the corn coating surface, displaying domains of relatively high, intermediate,

and low adhesion. Red circles indicate regions where FD curves were taken for (A), (B) and (C) respectively.

Chemical Mapping and Nonnegative Matrix Factorization Analysis

To understand whether chemical segregation is the driving force for the observed adhesion domains in Figure 1, the chemical composition of each coating was mapped on a 50 μm × 50 μm area using ToF-SIMS.[26] According to bulk Attenuated Total Reflection Fourier Transform Infrared Spectroscopy (ATR FTIR) analysis (Figures S3 and Figure S4 in Supporting Information), polymer matrices show high variation of the chemical groups presented. Meanwhile, the spectra of the coatings with the active component clearly contain the same peaks, see Figure S3 and Figure S4 in Supporting Information. This points to the fact that the active ingredient was the same for all three coatings while the polymers were distinctively different. These insights are useful for the further interpretation of the ToF-SIMS data.

Mass spectra were collected in negative ion mode with high spectral resolution to separate isobaric overlap from multiple constituents. The full scan ToF-SIMS mass spectra over the 50 μm × 50 μm area chemical maps for each coating is shown in Figure S5 in Supporting Information. Since each map consist of 16,384 individual spectra it is roughly ~0.5 GB in size. This is challenging for analysis and we utilized data processing methods to decompose these large data sets into chemical components that share common features. Nonnegative Matrix Factorization (NMF), groups data with many attributes (i.e peaks in spectra) and returns decomposed spectra with nonnegative peaks that are easily interpreted. The mass spectra that comprise ToF-SIMS maps are then represented as a linear mixtures of a given number of spectra. Thus, NMF decomposition yields these spectra (referred to as endmembers) as well as maps of the corresponding decomposition coefficients (commonly referred to as abundance maps). With this procedure, we expect individual components of a seed coating to have distinct spectra which are then mixed according to the ratio of these components within the area used for the generation of secondary ions during a single measurement. Considering these assumptions, NMF decomposition is well-suited for analysis of ToF-SIMS maps and has been demonstrated as effective on interpreting complex sample spectra.[26] In this case, endmembers reflect spectra of individual components of a mixture while abundance maps reflect the distribution of aforementioned components over the field of view. In this light, we refer to the abundance maps generated by NMF as chemical maps.

Here, NMF was applied to the ToF-SIMS spectra, and the NMF decomposition into three components is shown in Figure 2. As can be seen in Figure 2, while the NMF analysis on the three coatings (A, B, and C) was done independently, individual components share similar features across the samples. For example, the first component is almost identical for all three coatings (Figure 2A – B), containing significant amounts of Cl^{35-}, Cl^{37-}, CN^- or $C_2H_2^-$, S^-, HS^-, $C_2H_2S^-$ and CNO^- ions which is consistent with chlorine and sulfur-containing groups of the active compounds (see pages S3 – 35 in Supporting Information); and nearly disappears from the mass spectra in polymer matrices. Note that this finding is in good agreement with the results of bulk ATR FTIR analysis (Figure S3 and Figure S4 in Supporting Information). Therefore, we designate this as the active component. The regions corresponding to all components are shown in Figure 3, where the active compound, in red, covers a significant portion of the sampled area. The second component (Figure 2D – F) varies between all three coatings, but in all cases contains strong O^- and OH^- peaks; we designate this as the oxygen-rich component and is represented in green in Figure 3. The third component (Figure 2G – I) shows strong peaks associated with hydrocarbons (C_2H^- and $C_2H_2^-$)

and carbon atoms and clusters (C, C_2^-, C_3^-, C_4^-) and we designate this as the hydrocarbon-rich component and is displayed in blue in Figure 3.

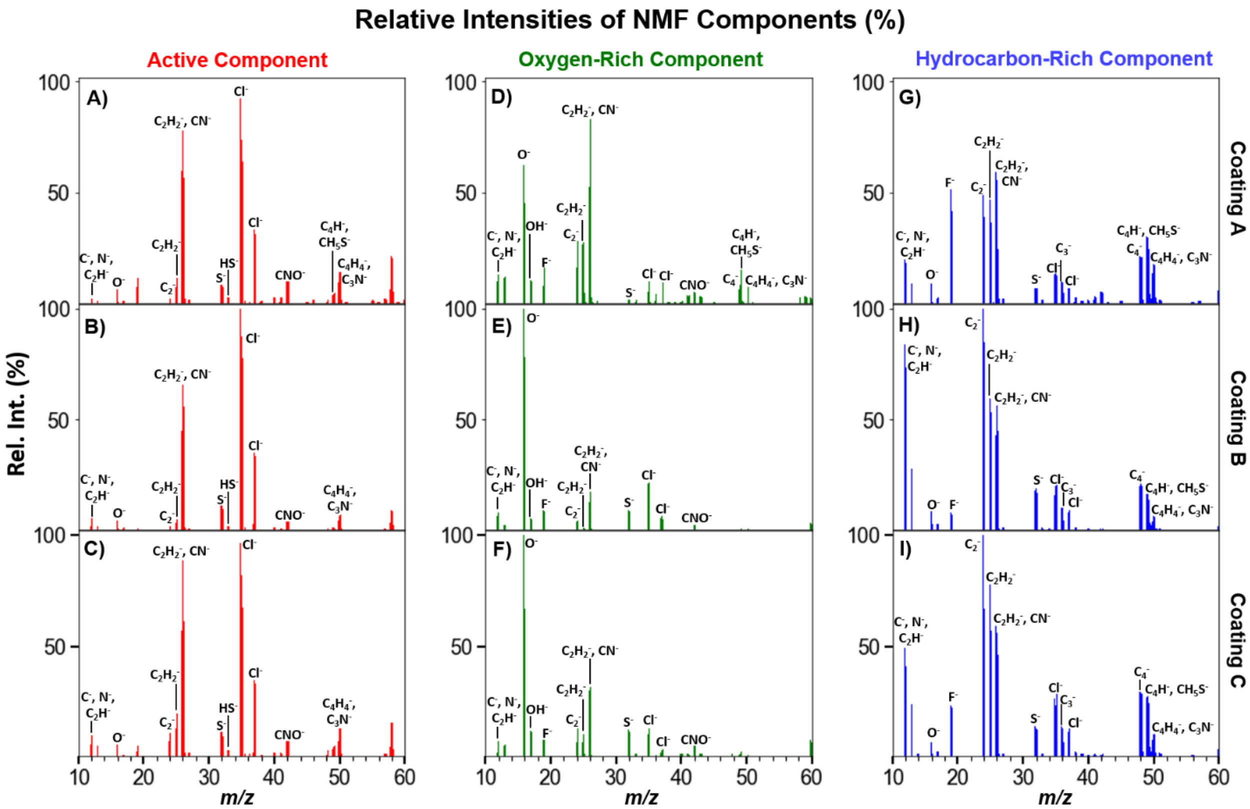

Figure 2. NMF components of the ToF-SIMS spectra from the corn seed coatings. (A)-(C) The active component from coating A, B, and C respectively. (D)-(F) The oxygen-rich component from coating A, B, and C respectively. (G)-(I) The hydrocarbon-rich component from coating A, B, and C respectively.

In Figure 3, the ToF-SIMS analysis of the three coatings shows varying spatial distribution of the three components (red, green, and blue). Coating A shows much finer domain segregation of the active compound in the polymer. Regions corresponding to oxygen-rich (green) and hydrocarbon-rich (blue) components appear together for coatings A and B and have similar shapes. In contrast, coating C has extended oblong domains of the oxygen-rich component that do not coincide with the hydrocarbon-rich domains.

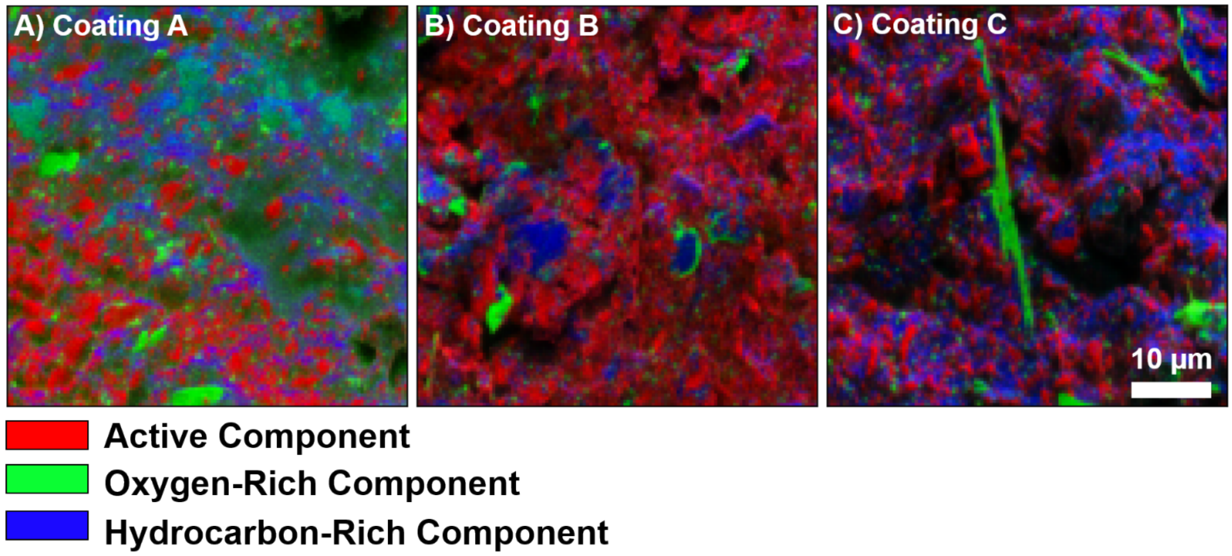

Figure 3. Representative chemical maps of the corn seed coatings supported by glass substrates obtained via ToF-SIMS. The scale bar of 10 μm is the same for all maps. NMF analysis of ToF-SIMS data distinguished three major components contributing to the overall ToF-SIMS signal. The distribution of these components within 50 μm × 50 μm areas on the coatings are shown in red (associated with the active component), green (associated with the oxygen-rich component), and blue (associated with the hydrocarbon-rich component). The mass spectra for each component for all the coatings are displayed above in Figure 2. A) Representative chemical map from coating A. B) Representative chemical map from coating B. C) Representative chemical map from coating C.

Relating Seed Coating Adhesion and Chemistry

Figure 4 correlates the adhesion maps and spatial distribution of the NMF components from the ToF-SIMS analysis. Adhesion and chemical maps have comparable length scales; however, these data were acquired on different areas since ToF-SIMS is a destructive technique. Examination of the chemical maps in Figure 3 reveals that coverage of the active component (red) is almost the same for all three coatings which is confirmed by ATR FTIR (Figure S3 in Supporting Information) suggesting that the active component has intrinsically low adhesion. Since inorganic fillers do not appear on the surface, and the ToF-SIMS spectra did not show metallic ions, SiO^- and $SiOH^-$ ions, and ions associated with TiO_2, we conclude that the choice of the polymer is the most influential factor for adhesion. The relationship between mechanical properties and chemical composition at the microscale corroborates the observed macroscopic properties and can guide design for improved corn seed coatings. Inorganic fillers do not contribute to the adhesion and the active component promotes lower adhesion. While the polymer matrices are only a fraction of the overall compositions, the coatings behave in agreement with the polymer thermal properties and with polymer chemical maps (oxygen-rich and hydrocarbon components). Therefore, it seems that the polymer matrices are responsible for higher adhesion.

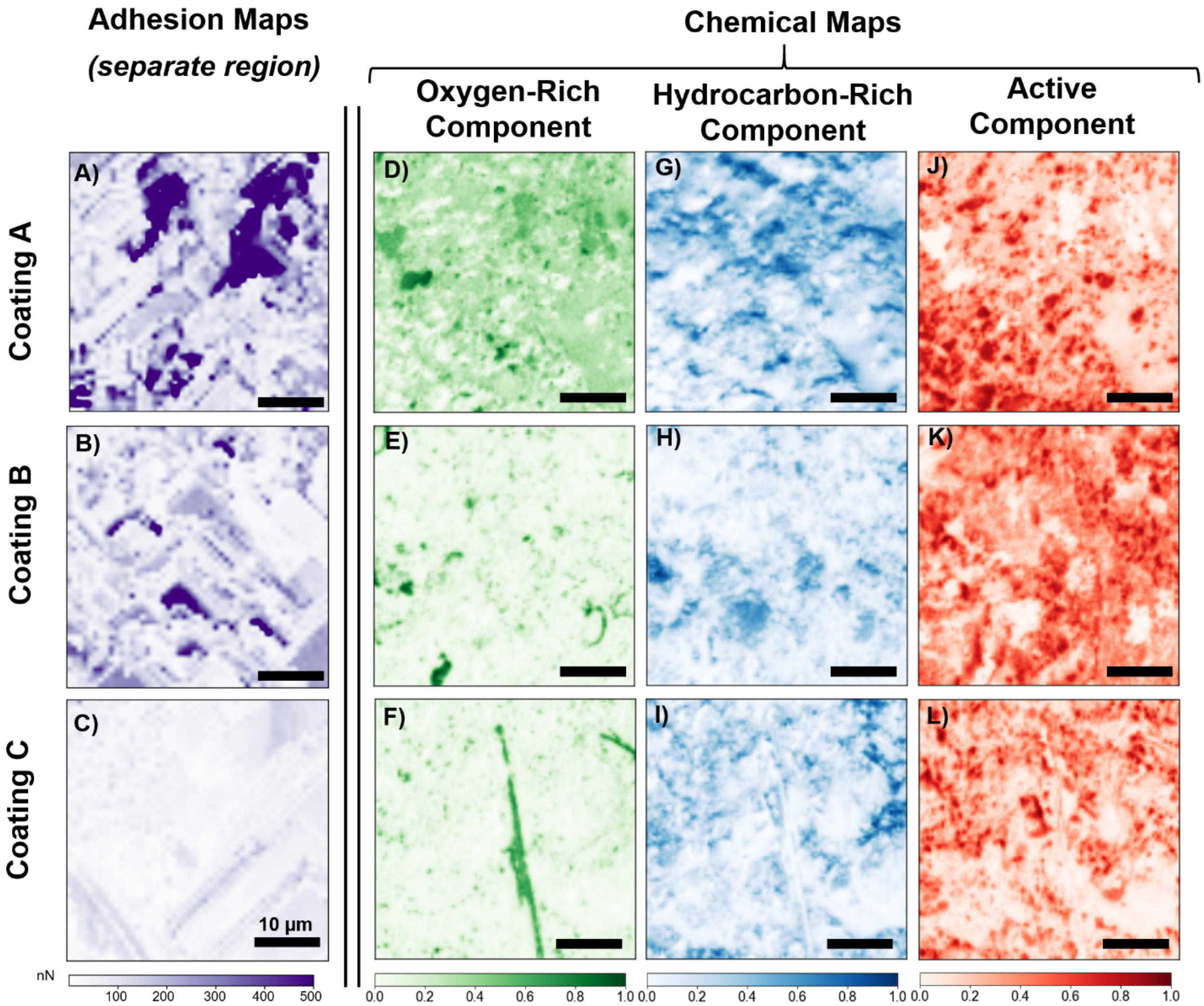

Figure 4. Representative adhesion and chemical maps (separated by component) for all three coatings are compared. The adhesion maps were obtained via AFM force volume mapping and the chemical maps were obtained with NMF analysis of ToF-SIMS. The scale bar of 10 μm is the same for all maps and note that the chemical maps have been reduced to 40 μm × 40 μm to easily compare with the 40 μm × 40 μm adhesion maps. A) Representative adhesion map from the surface of coating A. B) Representative adhesion map from the surface of coating B. C) Representative adhesion map from the surface of coating C. D) Representative chemical map of the ToF-SIMS oxygen-rich component from coating A. E) Representative chemical map of the ToF-SIMS oxygen-rich component from coating B. F) Representative chemical map of the ToF-SIMS

oxygen-rich component from coating C. G) Representative chemical map of the ToF-SIMS hydrocarbon-rich component from coating A. H) Representative chemical map of the ToF-SIMS hydrocarbon-rich component from coating B. I) Representative chemical map of the ToF-SIMS hydrocarbon-rich component from coating C. J) Representative chemical map of the ToF-SIMS active component from coating A. K) Representative chemical map of the ToF-SIMS active component from coating B. L) Representative chemical map of the ToF-SIMS active component from coating C.

Conclusions

In this work, we illustrate an analytical approach to address seed flow challenges in the agricultural industry, rooted in microscale analysis of the coatings. The local chemical composition of multicomponent polymer coatings, used in agrochemical manufacturing, were examined with ToF-SIMS and correlated with local adhesive properties using AFM force volume mapping. We found that the relative adhesion trend matches the trend in the coated seed flowability observed in industry. Likewise, the non-uniform distribution of local chemical groups designated as active, oxygen-rich, and hydrocarbon-rich components were observed. Using data analytics on the correlated multimodal imaging data sets, we were able to conclude that the oxygen-rich and the hydrocarbon-rich components follow the adhesion trend. This suggest that, unlike previously thought, the active component of the seed coating does not contribute to adhesion. Overall, it is driven by the choice of the polymer matrix which is paramount in controlling the microscale distribution of chemistry, and therefore overall flowability. The combination of AFM force volume mapping, ToF-SIMS chemical mapping, and data analytical methods developed here can be practically applied to a wide variety of investigations of soft material systems including improving agrochemical formulation to advance seed coating technology.

Materials and Methods

Coating Samples

The coatings included commercially available ingredients and primarily consisted of fungicides and insecticides (active ingredients), polymers and waxes, and inorganic fillers. The polymers and waxes with inorganic fillers, designated as polymer matrix, varied between coatings. We designate samples consisting of the polymer matrices mixed with the active ingredients as coating A, B, and C. The complete commercially available information on the coating compositions is presented in Supporting Information. Table S1 contains information for coating A, Table S2 contains information for coating B, and Table S3 contains information for coating C. The coatings were mixed and applied using standard agricultural procedures.[15,27-29] All the coatings were examined on a commercially available Indium Tin Oxide (ITO) coated glass surface (Bruker, Billerica, MA) to eliminate additional sources of error such as inhomogeneity in the mechanical properties of the corn seeds. In addition, polymer matrices for all three coatings (without active ingredients) have been deposited in the same manner and analyzed as well.

AFM Adhesion Mapping

Force volume maps were obtained with a MPF3D AFM (Asylum Research, Santa Barbra, CA). Colloidal probes (Novascan Technologies, Inc, Ames, IA) were used for force volume mapping with 5 μm borosilicate spheres. All tips were calibrated prior to experiment and were found to have 6 - 7 N/m spring constants. Force volume maps were conducted over a 40 μm × 40 μm areas consisting of a resolution of 50 × 50 points. FD curves were collected at each point for a total of 2,500 curves. The relative adhesion was determined by extracting the pull-off force *via* a Python script.

ToF-SIMS

Chemical maps and mass spectra were obtained using ToF-SIMS.5-NSC (Ion-TOF, Chestnut Ridge, NY) equipped with a Bi_3^+ primary ion gun and a Cs^+ sputtering source. The sputtering source was operated at 1 keV with a current of 75 nA. Identification of the secondary ions was performed in high spectral resolution mode. The mass resolution for a high spectral mode is 10000 $M/\Delta M$. The images were collected with a resolution of 128 × 128 points across a 50 μm × 50 μm imaging area from six samples: coatings A, B and C and corresponding polymer matrices (containing inorganic filler). Chemical maps consisted of a mass spectrum at each spatial pixel containing a total of 16,384 spectra. The chemical maps and the associated mass spectra were acquired in high spatial resolution mode, with the spatial resolution of 400 nm, beam energy of 30 keV, current of 0.48 nA, and spectral resolution of approximately 0.5 Da. NMF was used on the ToF-SIMS data to extract the major chemical contributors from the chemical maps. Using SurfaceLab (Ion-ToF, Chestnut Ridge, NY), NMF was done performed on mass spectra peaks between 0 – 500 m/z, with the criteria that peak exceeds 100 counts. The NMF decomposition score was 0.61, 0.54 and 0.63 for coatings A, B and C, respectively. As a result, for each composition each pixel on a map was assigned with three NMF coefficients corresponding to three components.

AUTHOR INFORMATION

Corresponding Author

*Author to whom correspondence should be addressed.

Olga S. Ovchinnikova

Center for Nanophase Materials Sciences

Oak Ridge National Laboratory

1 Bethel Valley Rd

Oak Ridge TN, 37831-6493

ovchinnikovo@ornl.gov

Author Contributions

The manuscript was written through contributions of all authors. All authors have given approval to the final version of the manuscript. ‡These authors contributed equally.

ACKNOWLEDGMENT

This manuscript has been authored by UT-Battelle, LLC, under Contract No. DE-AC0500OR22725 with the U.S. Department of Energy. The United States Government retains and the publisher, by accepting the article for publication, acknowledges that the United States Government retains a non-exclusive, paid-up, irrevocable, world-wide license to publish or reproduce the published form of this manuscript, or allow others to do so, for the United States Government purposes. The Department of Energy will provide public access to these results of federally sponsored research in accordance with the DOE Public Access Plan (http://energy.gov/downloads/doe-public-access-plan). This research was conducted at the Center for Nanophase Materials Sciences, which is a DOE Office of Science User Facility. N.G. and S.M. were supported by Syngenta Crop Protection.

ABBREVIATIONS

AFM, Atomic Force Microscopy; ToF-SIMS, Time of Flight Secondary Ion Mass Spectrometry; ITO, Indium Tin Oxide; FD, force distance; T_g, glass transition temperature; T_m, melting temperature; NMF, Nonnegative Matrix Factorization.

Supporting Information Available:

This document contains commercially available information about the composition and further analysis of the corn seed coatings presented herein. For all coating types we show ATR FTIR, topography and roughness obtained with AFM, and details related to NMF analysis of ToF-SIMS chemical maps. (PDF). This material is available free of charge *via* the Internet at http://pubs.acs.org.

REFRENCES

(1) Halecky, A.; Ren, N.; Lu, J.; Jane Q, W.; Lockwood, F. E. *Pesticide Formulation and Delivery Systems: Emerging Trends Building on a Solid Foundation, ASTM STP1595* **2016**, *36*, 183-201.
(2) Nuyttens, D.; Devarrewaere, W.; Verboven, P.; Foque, D. *Pest Manag Sci* **2013**, *69*, 564-575.
(3) Plinke, M. A. E.; Maus, R.; Leith, D. *American Industrial Hygiene Association Journal* **1992**, *53*, 325-330.
(4) Accinelli, C.; Abbas, H. K.; Shier, W. T. *Crop Improv.* **2018**, *32*, 318-330.
(5) Pedrini, S.; Merritt, D. J.; Stevens, J.; Dixon, K. *Trends Plant Sci* **2017**, *22*, 106-116.
(6) Yao, Y.; Hou, J. H.; Xu, Z.; Li, G.; Yang, Y. *Advanced Functional Materials* **2008**, *18*, 1783-1789.
(7) Atares, L.; Chiralt, A. *Trends in Food Science & Technology* **2016**, *48*, 51-62.
(8) Krishnamoorthy, V.; Rajiv, S. *ACS Sustainable Chemistry & Engineering* **2017**, *5*, 146-152.
(9) Bao, X. Y.; Ali, A.; Qiao, D. L.; Liu, H. S.; Chen, L.; Yu, L. *Acta Polymerica Sinica* **2015**, 1010-1019.
(10) Karami, S.; Sabzalian, M. R.; Rahimmalek, M.; Saeidi, G.; Ghasemi, S. *Crop Protection* **2017**, *98*, 267-275.
(11) Ashraf, M.; Foolad, M. R. In *Advances in Agronomy, Vol 88*, Sparks, D. L., Ed.; Elsevier Academic Press Inc: San Diego, 2005, pp 223-271.
(12) Madsen, M. D.; Davies, K. W.; Boyd, C. S.; Kerby, J. D.; Svejcar, T. J. *Restoration Ecology* **2016**, *24*, S77-S84.
(13) Sidhu, H.; Monono, E.; Bora, G.; Wiesenborn, D. *Agricultural Research* **2017**, *6*, 347-358.
(14) Robani, H. *HortTechnology* **1994**, *4*, 104-105.

(15) Accinelli, C.; Abbas, H. K.; Little, N. S.; Kotowicz, J. K.; Mencarelli, M.; Shier, W. T. *Crop Protection* **2016**, *89*, 123-128.
(16) Nuyttens, D.; Devarrewaere, W.; Verboven, P.; Foque, D. *Pest Management Science* **2013**, *69*, 564-575.
(17) Jones, R.; Pollock, H. M.; Cleaver, J. A. S.; Hodges, C. S. *Langmuir* **2002**, *18*, 8045-8055.
(18) Jones, R.; Pollock, H. M.; Geldart, D.; Verlinden-Luts, A. *Ultramicroscopy* **2004**, *100*, 59-78.
(19) Jones, R. *Granular Matter* **2003**, *4*, 191-204.
(20) Jones, R.; Pollock, H. M.; Geldart, D.; Verlinden, A. *Powder Technology* **2003**, *132*, 196-210.
(21) Pedrini, S.; Merritt, D. J.; Stevens, J.; Dixon, K. *Trends Plant Science* **2017**, *22*, 106-116.
(22) Zhou, E.; Cong, J. Z.; Hashimoto, K.; Tajima, K. *Advanced Materials* **2013**, *25*, 6991-6996.
(23) Radmacher, M.; Fritz, M.; Cleveland, J. P.; Walters, D. A.; Hansma, P. K. *Langmuir* **1994**, *10*, 3809-3814.
(24) Pimpang, P.; Zoolfakar, A. S.; Wongratanaphisan, D.; Gardchareon, A.; Nguyen, E. P.; Zhuiykov, S.; Choopun, S.; Kalantar-zadeh, K. *Journal of Physical Chemistry C* **2013**, *117*, 19984-19990.
(25) Tsui, O. K. C.; Wang, X. P.; Ho, J. Y. L.; Ng, T. K.; Xiao, X. D. *Macromolecules* **2000**, *33*, 4198-4204.
(26) Ievlev, A. V.; Belianinov, A.; Jesse, S.; Allison, D. P.; Doktycz, M. J.; Retterer, S. T.; Kalinin, S. V.; Ovchinnikova, O. S. *Scientific Reports* **2017**, *7*, 17099.
(27) United States, 1999.
(28) Pasha, M.; Hare, C.; Ghadiri, M.; Gunadi, A.; Piccione, P. M. *Chemical Engineering Research & Design* **2017**, *120*, 92-101.
(29) Kage, H.; Takahashi, T.; Yoshida, T.; Ogura, H.; Matsuno, Y. *Powder Technology* **1996**, *86*, 243-250.

TABLE OF CONTENTS (TOC) GRAPHIC

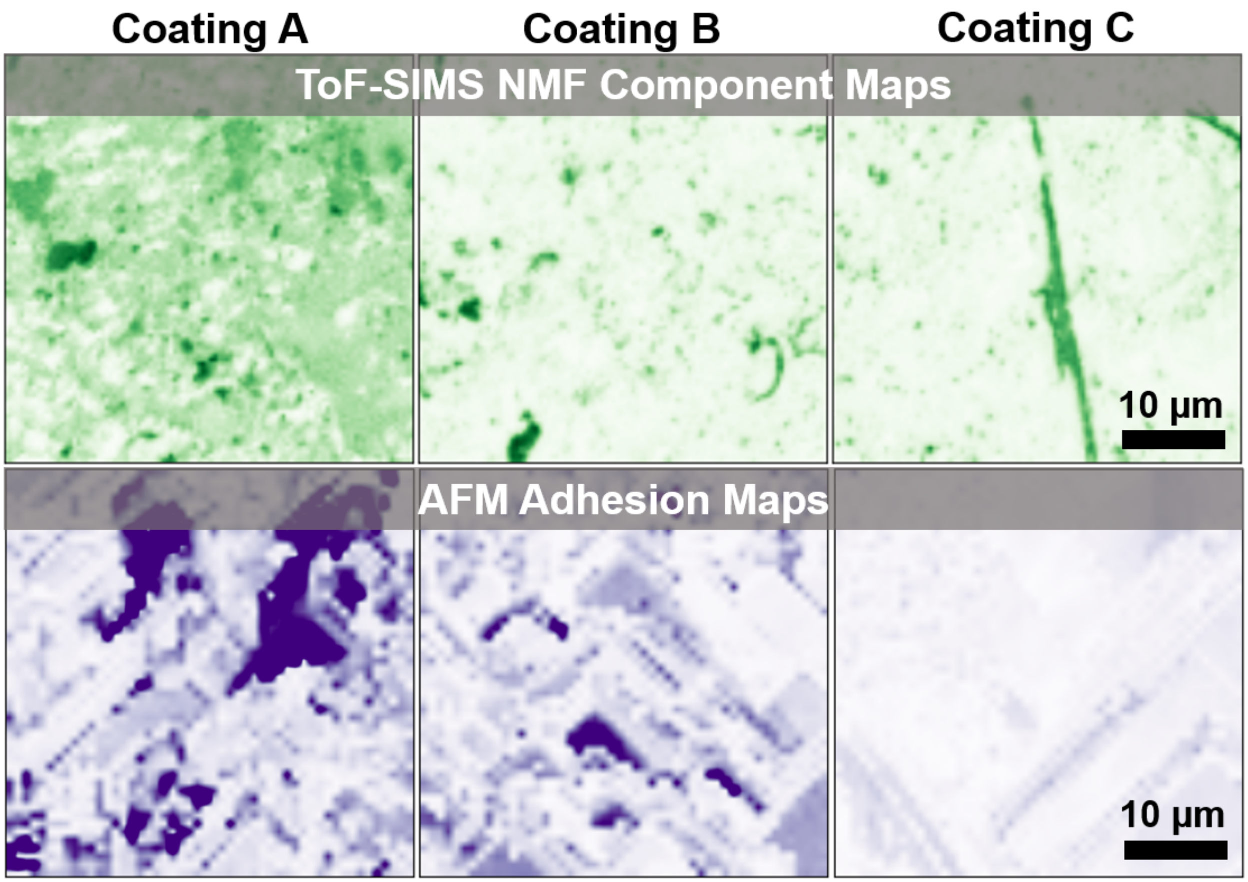
Coating A
Coating B
Coating C
ToF-SIMS NMF Component Maps
10 µm
AFM Adhesion Maps
10 µm